PCCP

PAPER

View Article Online
View Journal | View Issue

Cite this: *Phys. Chem. Chem. Phys.*, 2018, **20**, 30437

The stability and unexpected chemistry of oxide clusters†

Xiaohu Yu,*[ab] Artem R. Oganov,[acd] Qiang Zhu,[e] Fei Qi[af] and Guangrui Qian[e]

Received 4th June 2018,
Accepted 9th November 2018

DOI: 10.1039/c8cp03519a

rsc.li/pccp

Using evolutionary structure prediction and *ab initio* thermodynamics, we determine stable compositions and structures of small Ce_mO_n and Fe_mO_n clusters at realistic temperatures and oxygen pressures. We use second energy differences as the criterion determining clusters of particular stability (''magic'' clusters), whereas HOMO–LUMO gaps are used to gauge chemical inertness – *i.e.* the ability of a cluster to survive in a complex chemical environment. We find that, similar to atomic nuclei (which are clusters made of neutrons and protons), compositional space of two-component clusters also has ridges and islands of stability, surrounded by sea of instability. Long ridges of stability correspond to stoichiometric compositions – *e.g.*, $(CeO_2)_k$, $(Ce_2O_3)_k$, $(FeO)_k$, $(Fe_2O_3)_k$ and $(Fe_3O_4)_k$ series of clusters, while ''islands of stability'' can have very unexpected compositions. For example, at room temperature and ambient atmosphere, superoxidized Fe_4O_8 clusters will be dominant among the Fe_4O_n clusters. We emphasize that stability is dictated not only by closed geometric and electronic shells, but also by magnetism.

Nanoclusters possess a wide variety of physical and chemical properties, and peculiar electronic and geometric structures. However, their small size hampers full structural characterization by experimental techniques.[1] In fact, most of the structural models are generally inferred indirectly, often with the aid of theoretical approaches.[2] It was found that nanoclusters of certain sizes and shapes, known as 'magic clusters', possess enhanced stability. Such magic clusters can serve as building blocks to assemble bulk materials.[3] Their stability can be either structural (closed atomic shell – when atoms form a complete symmetric shell, *e.g.* icosahedral[4]) or electronic (due to closed electronic shell, precise electron count, or aromaticity). Stability due to a closed electronic shell is found, *e.g.*, in alkali metal clusters, which are well described by the jellium model[5,6] and behave as ''superatoms'' with collective electronic orbitals that form electronic shells. In addition, new models of aromaticity have been put forward to explain enhanced stability of certain metal clusters, such as Al_n and Cr_n,[7] and antiferromagnetism was also found to play an important role in stabilizing such clusters as Ti_8O_{12}.[8] Recently, it was reported that for the cage $Fe_{12}O_{12}$ cluster, the antiferromagnetic state is much more stable (by $\sim$1.25 eV) than ferromagnetic.[9]

Full understanding of the intrinsic factors, which determine the stability of oxide clusters, is still lacking. The first step to this goal is to understand the relationship between stability of such clusters and chemical variables, such as composition and chemical environment. In this paper, we tackle this question by a systematic study of stable structures of Ce_mO_n and Fe_mO_n clusters under realistic conditions using evolutionary structure prediction. We identify magic Ce_mO_n and Fe_mO_n clusters using thermodynamic criteria and correlate stability with their electronic structure. Conclusions drawn from such study are applicable to other oxide clusters.

Cerium and iron oxide clusters play an important role in catalysis and environmental remediation. There have been a number of studies dedicated to investigating the geometric and electronic structures of transition metal oxide nanoclusters: neutral Ce_mO_{2m-x} ($m \leq 4$, $0 \leq x \leq m$)[10,11] and Ce_mO_{2m} (m = 1–6)[12,13] clusters. Li *et al.*[10] found that Hubbard's U parameter strongly affects the electronic structure of oxygen-deficient Ce_nO_{2n-1} clusters. Structures of Fe_mO_n,[14–19] $(FeO)_k$,[20] and $(Fe_2O_3)_k$[21,22] clusters have also been studied. Ding *et al.*,[21] studying cage and noncage $(Fe_2O_3)_k$ (k = 2–6, 10) cluster, found that global minima have noncage structures in most cases. Recently, it was reported that the precise magnetic state of clusters has small

[a] *Moscow Institute of Physics and Technology, 9 Institutskiy Lane, Dolgoprudny, Moscow Region, 141700, Russia. E-mail: yuxiaohu950203@126.com*
[b] *Institute of Theoretical and Computational Chemistry, Shaanxi Key Laboratory of Catalysis, School of Chemical & Environment Sciences, Shaanxi University of Technology, Hanzhong 723000, China*
[c] *Skolkovo Institute of Science and Technology, 3 Nobel St., 143026 Moscow, Russia*
[d] *International Center for Materials Discovery, Northwestern Polytechnical University, Xi'an 710072, China*
[e] *Department of Geosciences, Stony Brook University, Stony Brook, New York 11794, USA*
[f] *School of Electronic Engineering, Xidian University, Xi'an, Shaanxi, 710071, China*

† Electronic supplementary information (ESI) available: Magnetic moments and HOMO–LUMO gaps of Fe_4O_n and Ce_4O_n clusters, spin density distribution in Ce_4O_n and Fe_4O_n clusters, magic clusters of Ce_mO_n and Fe_mO_n and coordinates of magic clusters. See DOI: 10.1039/c8cp03519a

influence on the geometric structure from investigating neutral $(Fe_2O_3)_k$ (k = 1–5) clusters,[22] and evolution of the structure of Fe_2O_3 clusters from the smallest size to nanometer-sized Fe_2O_3 particles was studied.[23] López *et al.*[24] studied the structure and electronic properties of iron oxide clusters using the GGA+U method. Palotás *et al.*[25] demonstrated the adequacy of GGA+U in their study of iron oxide clusters.

Structure predictions were performed using the *ab initio* evolutionary algorithm USPEX,[26] which has been successfully applied to various bulk materials (*e.g.*, ref. 27), 2D structures,[28] nanoclusters[29,30,41] and polymers.[31] In our nanoparticle structure predictions, an initial population of structures is produced using random symmetric generator.[27] All structures were relaxed and then ranked by energy, with lower-energy 60% of structures selected as parents for the new generation (by specially designed variation operators, such as heredity, permutation and soft-mutation). According to our tests, spin states play an important role in determining the stability of Fe_mO_n clusters and rather little role for Ce_mO_n clusters – therefore, a spin mutation operator was used for Fe_mO_n clusters and the initial magnetic moments were randomly assigned to iron atoms at the stage of producing the first generation of structures. Calculations proceeded until the lowest-energy structure remained unchanged for a sufficiently large number of generations, as was done in the previously published papers.[8,9] During global optimization, all structures were relaxed using the all-electron-projected-augmented wave method as implemented in the Vienna *ab initio* simulation package (VASP).[32,33] In these calculations, clusters were surrounded by a 12 Å thick vacuum. In order to decrease the computational cost, we used the Perdew–Burke–Ernzerhof (PBE) functional, with a Hubbard-like U correction (DFT+U), in the form developed by Dudarev *et al.*,[34] to account for the self-interaction error inherent to semilocal functionals such as PBE. We used an effective $U_{eff} = U - J$ value of 5 eV[10,11,35,36] for the Ce atom and 4 eV for the Fe atom,[25,37–39] which have been shown to be a good choice for an accurate description of both the atomic and electronic structure of ceria and iron oxide. The energy cutoff for the plane-wave expansion was set to 400 eV. Structure relaxations were performed until the Hellmann–Feynman force on each atom became less than 0.001 eV Å^{-1}. Vibrational frequency calculations were performed to check that the predicted structures have no imaginary frequencies. The hybrid functional (HSE06)[40–42] was also used to test the magnetic moments and HOMO–LIMO gaps of Ce_mO_n and Fe_mO_n clusters. It was found that the effect of different methods on the magnetic moments of Ce_mO_n and Fe_mO_n clusters is small, while the effect of different methods on the HOMO–LUMO gaps of Ce_mO_n and Fe_mO_n clusters is large, and the detailed test results are listed in Tables S1, S2, and Fig. S1, S2 in the ESI.† However, the results of HOMO–LUMO gaps agree well with previous results: hybrid functionals usually predict a larger gap than the DFT methods.[43] One can easily see that stoichiometric Fe_mO_n and Ce_mO_n clusters have larger HOMO–LUMO gaps than other clusters for both different methods from Fig. S1 and S2 (ESI†). Note that there are no experimental HOMO–LUMO gaps for nonstoichiometric Ce_mO_n and Fe_mO_n clusters to compare with our DFT+U gaps.

We considered a wide range of Ce_mO_n and Fe_mO_n cluster sizes: m from 1 to 10 and n in the n = 0–14 and n = 0–20 ranges for small (m = 1–6) and larger ($m > 6$) clusters, respectively. For each stoichiometry, the energy was minimized with respect to both geometry and spin state.

We evaluated the Gibbs free energy[44–47] as $\Delta G_f(T,p_{O_2}) = F_{M_mO_n}(T) - F_{M_m}(T) - n\mu_O(T,p_{O_2})$, where $F_{M_mO_n}(T)$ and $F_{M_m}(T)$ are the Helmholtz free energy of the M_mO_n (Ce_mO_n and Fe_mO_n) and the pristine M_m (Ce_m and Fe_m) clusters (at their ground state with respect to geometry and spin), respectively, and $\mu_O(T,p_{O_2})$ is the chemical potential of oxygen. In equilibrium with molecular O_2 gas, $\mu_O(T,p_{O_2})$ is expressed as $\mu_O(T,p_{O_2}) = 1/2[E_{O_2} + \mu_{O_2}(T,p^0) + k_BT\ln(p/p^0)]$, where p^0, k_B, and p are the standard atmospheric pressure, Boltzmann constant, and oxygen partial pressure, respectively. E_{O_2} was obtained from a spin-polarized calculation. The $\mu_{O_2}(T,p^0)$ term includes contributions from spin flips, vibrations and rotations of O_2 molecules at atmospheric pressure and was taken from thermodynamic tables.[48] $k_BT\ln(p/p^0)$ is the contribution of temperature and O_2 partial pressure to the oxygen chemical potential. The phase diagram for each m was constructed by identifying the lowest-free-energy structures at each (T,p_{O_2}).

Fig. 1 shows the computed phase diagrams of Ce_4O_n and Fe_4O_n. Ambient conditions and lower temperature or higher oxygen pressure favor nonstoichiometric oxygen-rich clusters Ce_4O_n ($n > 8$) and Fe_4O_n ($n > 6$). In contrast, oxygen-deficient clusters are stabilized by high T and low p_{O_2}. Oxygen desorption

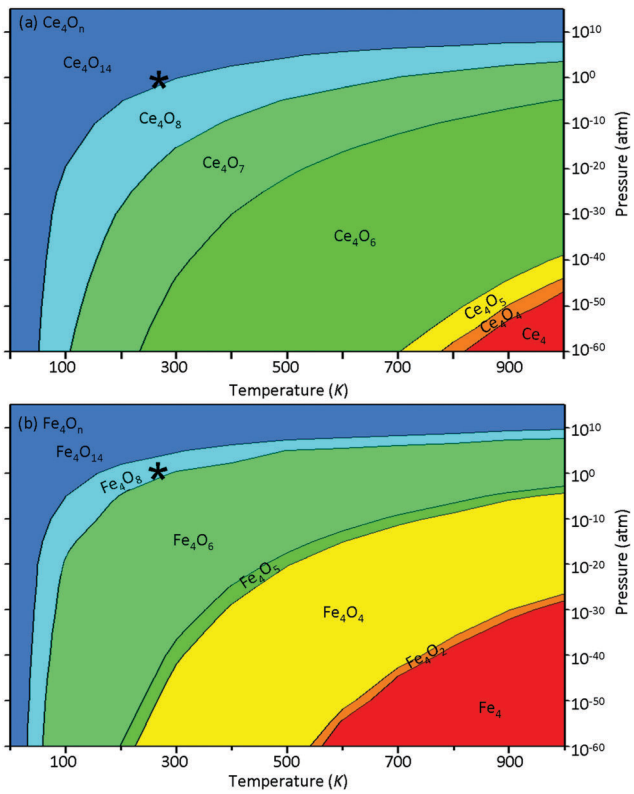

Fig. 1 Phase diagrams of Ce_4O_n (a) and Fe_4O_n (b) in an oxygen atmosphere. The star "*" shows standard conditions.

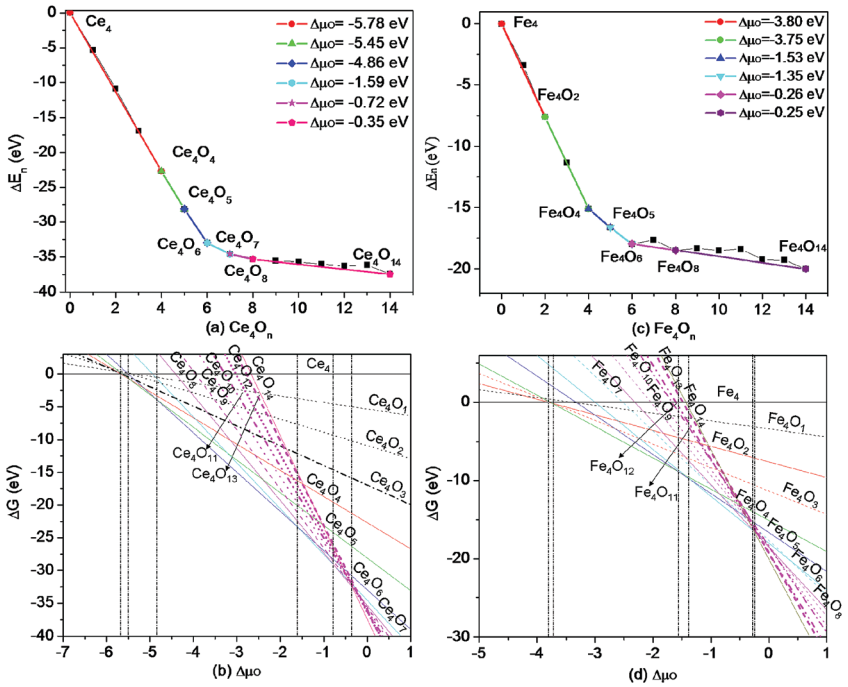

Fig. 2 (a) Convex hull and (b) phase diagram of Ce_4O_n (n = 0–14, number of oxygen atoms); (c) convex hull and (d) phase diagram of Fe_4O_n (n = 0–14) (solid line means stable cluster-refers to the phase diagrams [*i.e.* (b) and (d)]).

at high temperatures is easy to understand: oxygen gas has very high entropy, and its formation is favorable at sufficiently high temperatures. Existing experimental results for $(Fe_2O_3)_k$ and $(FeO)_k$ clusters are consistent with our predictions.[49–52] Free energies of formation of the most stable nonstoichiometric (a) Ce_mO_n ($n \neq 2m$) and (b) Fe_mO_n ($n \neq m$) clusters, relative to stoichiometric (a) Ce_mO_n ($n = 2m$) and (b) Fe_mO_n ($n = m$) clusters under several (T,p_{O_2}) conditions are shown in Fig. S3 (ESI†).

Spin density distribution in Ce_4O_n clusters is shown in Fig. S4 (ESI†). For Ce_4O_8 clusters, the ground state is singlet, while in Ce_4O_7 and Ce_4O_6 clusters there are two and four, respectively, unpaired electrons localized on f-orbitals – just as many as Ce^{3+} atoms. We found this to be a general trend: the Ce_nO_{2n} and Ce_nO_{2n-1} clusters are in singlet and triplet states, respectively. By changing T and partial pressure of oxygen, one can change the stoichiometry and magnetic state of clusters.

On the other hand, Fe_4 is ferromagnetic, Fe_4O_1 is ferrimagnetic, and the other lowest-energy Fe_4O_n clusters are all antiferromagnetic (Fig. S5 and S6, ESI†). Exchange interaction between non-neighboring magnetic ions that have the same oxidation state is known as the superexchange effect,[53] while the exchange interaction between non-neighboring magnetic ions with different oxidation states can be termed the double exchange effect.[54] Thus the ferrimagnetic state of Fe_4O_n clusters is induced by the competition between ferromagnetism (due to direct exchange) and antiferromagnetism (induced by superexchange or double exchange) – the latter wins in oxygen-rich clusters. For example, superexchange effect plays an important role in the antiferromagnetic Fe_4O_4 cluster with all four Fe atoms in the +2 oxidation state, while double exchange effect wins in the antiferromagnetic Fe_4O_5 cluster with two Fe atoms in the +2 oxidation state and other two Fe atoms in the +3 oxidation state. The structure of the Fe_4O_6 cluster is made of a tetrahedral Fe_4 core and six O atoms on each of the six edges of the tetrahedron – which agrees well with available experimental and theoretical results.[17] Our calculations show that spin state is a very important factor determining the stability of Fe_mO_n clusters (Fig. S6, ESI†).

Convex hulls and phase diagrams of Ce_4O_n and Fe_4O_n clusters are shown in Fig. 2. In the convex hulls (Fig. 2a and c), each of clusters is represented as a point, and the points corresponding to stable clusters form a convex hull. In the phase diagrams (Fig. 2b and d), each cluster is represented by a straight line which represents its Gibbs free energy as a function of the chemical potential of oxygen, and stable clusters are those that have the lowest Gibbs free energy at a certain range of chemical potentials. There are seven stable clusters appearing on the convex hull in Fig. 2a: Ce_4, Ce_4O_4, Ce_4O_5, Ce_4O_6, Ce_4O_7, Ce_4O_8 and Ce_4O_{14}, consistent with Fig. 1a and 2b. For Fe_4O_n clusters, there are six stable clusters (Fig. 2c and d): Fe_4, Fe_4O_2, Fe_4O_4, Fe_4O_5, Fe_4O_6, Fe_4O_8 and Fe_4O_{14}, consistent with Fig. 1b.

Another interesting feature is that nonstoichiometric Ce_mO_n ($n > 2m$) and Fe_mO_n ($2n > 3m$) clusters have peroxo- and superoxo-groups (*e.g.*, in Fe_4O_9 and Fe_4O_{12} – Fig. S7, ESI†), with peroxo-groups attached side-on $[Fe(O)_2]$ and superoxo-groups attached end-on (FeOO).[55] Recently, the same phenomenon was reported for Si_mO_n ($n > 2m$) clusters.[56] The thermodynamically favored excess of oxygen in nanoclusters is in sharp contrast with the bulk crystal, where the stoichiometric composition is strongly favored. In contrast to the nonstoichiometric clusters, stoichiometric clusters $(CeO_2)_k$ are always singlet (non-magnetic), while both the nonstoichiometric and stoichiometric Fe_mO_n clusters are antiferromagnetic or ferrimagnetic.

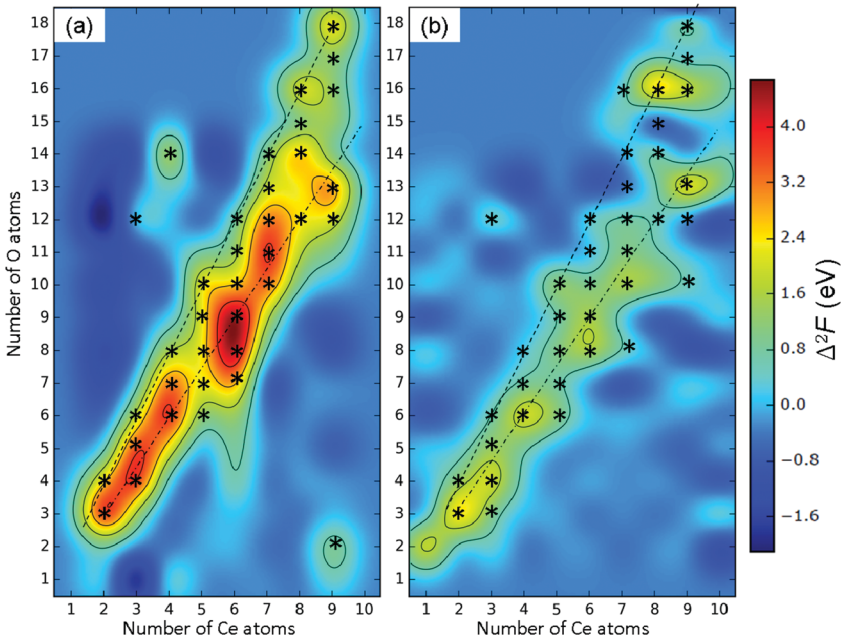

Fig. 3 Stability of Ce_mO_n clusters (shown by stars) determined by second energy differences (a) $\Delta^2F_m = F(Ce_{m-1}O_n) + F(Ce_{m+1}O_n) - 2F(Ce_mO_n)$ and (b) $\Delta^2F_n = F(Ce_mO_{n-1}) + F(Ce_mO_{n+1}) - 2F(Ce_mO_n)$. Clearly, $(CeO_2)_k$ and $(Ce_2O_3)_k$ clusters are doubly magic. This map shows ridges and islands of stability, surrounded by the "sea of instability", and allows one to find feasible and infeasible chemical transformations. For example, Ce_3O_{12} is a doubly magic cluster, but its synthesis requires simultaneous addition of six oxygen atoms to the nearest doubly magic cluster Ce_3O_6, which will be a rare process.

To evaluate the stability of clusters as a function of chemical composition, we considered the second energy difference defined from the energy of formation:

$$\Delta^2F_m = F(M_{m-1}O_n) + F(M_{m+1}O_n) - 2F(M_mO_n) \quad (1)$$

$$\Delta^2F_n = F(M_mO_{n-1}) + F(M_mO_{n+1}) - 2F(M_mO_n) \quad (2)$$

where the energy of formation is defined as:

$$F(M_mO_n) = E(M_mO_n) - mE(M) - 1/2nE(O_2) \quad (3)$$

$E(M_mO_n)$ is the energy of the M_mO_n cluster and $E(M)$ is the energy of a single metal atom. A positive second energy difference indicates a magic M_mO_n cluster: in this case, a homogeneous ensemble of identical clusters is stable against disproportionation by transfer of an atom from one cluster to another. Positiveness of Δ^2F with respect to both types of atoms indicates that the cluster is doubly magic – suggesting that it should be abundant, less reactive than neighboring clusters, and well defined in terms of its geometric and electronic structure. This language

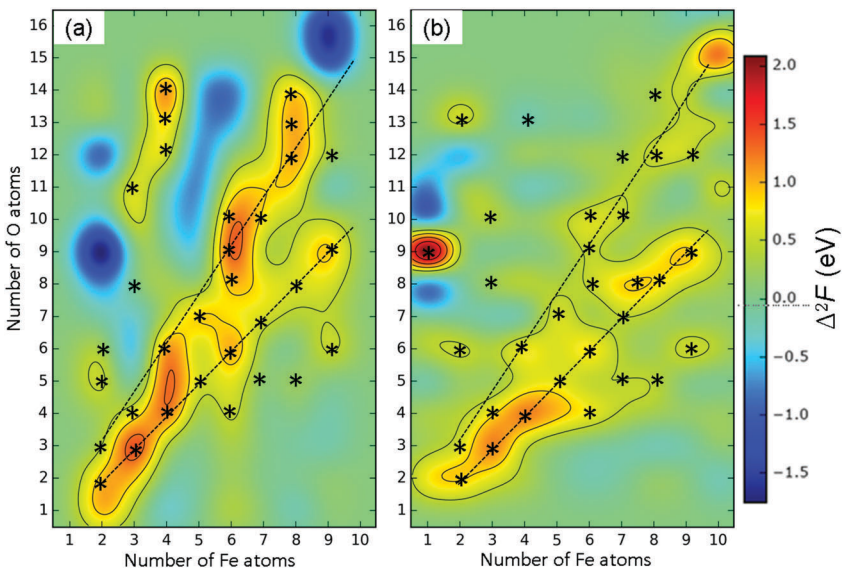

Fig. 4 Stability of Fe_mO_n clusters (shown by stars) as determined by second energy differences (a) $\Delta^2F_m = F(Fe_{m-1}O_n) + F(Fe_{m+1}O_n) - 2F(Fe_mO_n)$ and (b) $\Delta^2F_n = F(Fe_mO_{n-1}) + F(Fe_mO_{n+1}) - 2F(Fe_mO_n)$. Clearly, $(FeO)_k$, $(Fe_2O_3)_k$ and $(Fe_3O_4)_k$ clusters are doubly magic.

(singly magic and doubly magic clusters) is similar to the terminology used for describing stable atomic nuclei – singly magic have particular stability with respect to the number of either protons or neutrons, and doubly magic are stable with respect to both. In this language, our above consideration of stable Ce_4O_n and Fe_4O_n clusters with fixed numbers of metal atoms corresponds to finding singly magic clusters (with respect to the number of oxygen atoms). Adding stability with respect to the number of metal atoms indicates only Ce_4O_6, Ce_4O_7 and Ce_4O_8 clusters as doubly magic among all Ce_4O_n clusters – and only Fe_4O_4, Fe_4O_6 and Fe_4O_{13} among the Fe_4O_n clusters. Doubly magic clusters feature most prominently on the phase diagrams (Fig. 1).

Fig. 3 shows the second energy difference for Ce_mO_n clusters. Clusters with large positive second energy differences are particularly stable. We can clearly see that clusters in $(CeO_2)_k$ and $(Ce_2O_3)_k$ series are doubly magic, due to their electronic structure. It is well known that clusters with large gaps between the highest occupied molecular orbitals (HOMOs) and lowest unoccupied molecular orbitals (LUMOs) exhibit lower reactivity, because such clusters are more reluctant to either accept or donate an electron. Consequently, the HOMO–LUMO gap is a simple marker of less reactive, and consequently, chemically more stable clusters that have larger chances of surviving in complex chemical environments. As is well known, Ce atoms have two oxidation states, Ce^{3+} and Ce^{4+}, and clusters possessing only these states are expected to have large HOMO–LUMO gaps. In order to analyze the stability of $(CeO_2)_k$ and $(Ce_2O_3)_k$ clusters, we calculated the HOMO–LUMO gaps of stable clusters (Fig. 5a). The HOMO–LUMO gaps of $(CeO_2)_k$ clusters calculated using the GGA+U method are all between 1.50–2.30 eV, except CeO_2 (0.3 eV). The HOMO–LUMO gaps of $(Ce_2O_3)_k$ series are in the range 1.2–1.7 eV. Due to the stable Ce^{3+} state, Ce_nO_{2n-1} clusters also have large second energy differences and large HOMO–LUMO gaps (1.3–1.8 eV).

In one type of geometrically magic clusters, we find denser clusters similar to bulk crystal structures: for example, doubly magic clusters Ce_3O_4, Ce_6O_8, Ce_7O_{10}, Ce_8O_{14}, Ce_9O_{16}, and so on (Fig. S8, ESI†). In particular, the Ce_6O_8 cluster is the smallest octahedral cluster with exposed (111) facets and possesses unique d-orbital spherical aromaticity.[57] In experiments, transmission electron microscopy revealed nanoparticles of octahedral and cuboctahedral shapes, with (111) and (100) facets.[58] Another group of geometrically magic clusters cannot be represented as fragments of bulk structures, but still are characterized by high symmetry, for example: Ce_5O_6, Ce_5O_7, Ce_5O_8, Ce_6O_9, Ce_6O_{10}, Ce_7O_{11}, Ce_7O_{12}, Ce_9O_{12} and Ce_9O_{16} (Fig. S8, ESI†). Stable at high oxygen fugacities, the Ce_3O_{12} cluster is also doubly magic; its structure contains three peroxides O_2^{2-} adsorbed on the three terminal Ce atoms, two superoxides O_2^- occupying bridging positions between Ce atoms, and two oxide O^{2-} ions adsorbed above a three-hollow site and a Ce–Ce bridge.

Generally, the addition of O atoms to $(CeO_2)_n$ clusters leads to a decrease of the average oxygen binding energy (Fig. S9b and S11b, ESI†) and the formation of O–O bonds. Destabilization is signaled by positive values of the stepwise oxygen binding energy (Fig. S9a and S11a, dotted line, ESI†).

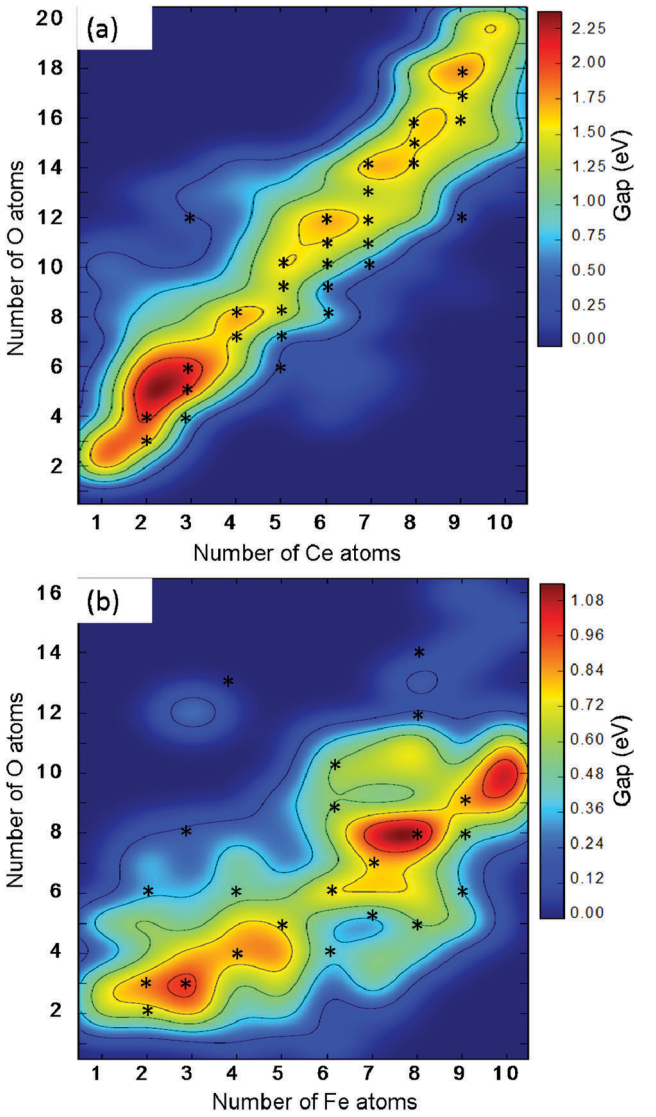

Fig. 5 HOMO–LUMO gap as a function of composition (a) Ce_mO_n (b) Fe_mO_n. The large ridge and small islands of stability can be easily seen.

Fig. 4 shows the second energy difference of Fe_mO_n clusters. We can see that clusters in $(FeO)_k$ and $(Fe_2O_3)_k$ series are stable. Fe has two oxidation states, Fe^{2+} and Fe^{3+}; and clusters based on these states are magic. For $(FeO)_k$ clusters, we have computed spin gaps as $\Delta_1 = -(\varepsilon_{HOMO}{}^{+} - \varepsilon_{LUMO}{}^{-})$ and $\Delta_2 = -(\varepsilon_{HOMO}{}^{-} - \varepsilon_{LUMO}{}^{+})$(+, spin up; −, spin down), corresponding to the energy required to move an electron from the HOMO of one spin to the LUMO of the other. Large positive values for both spin gaps can guarantee that the system is a stable magnetic and electronic state.[59,60] The spin gaps of $(FeO)_k$ (k = 3–10) are all positive (0.2–0.95 eV). $(Fe_2O_3)_k$ clusters also have a positive spin gap. $(Fe_3O_4)_k$ clusters are particularly stable among the Fe_mO_n clusters, as can be seen from their large Δ^2F, suggesting that $(Fe_3O_4)_k$ nanoparticles may better survive in chemically complex environments, and this can be attributed to the wide abundance of magnetite Fe_3O_4 in nature.

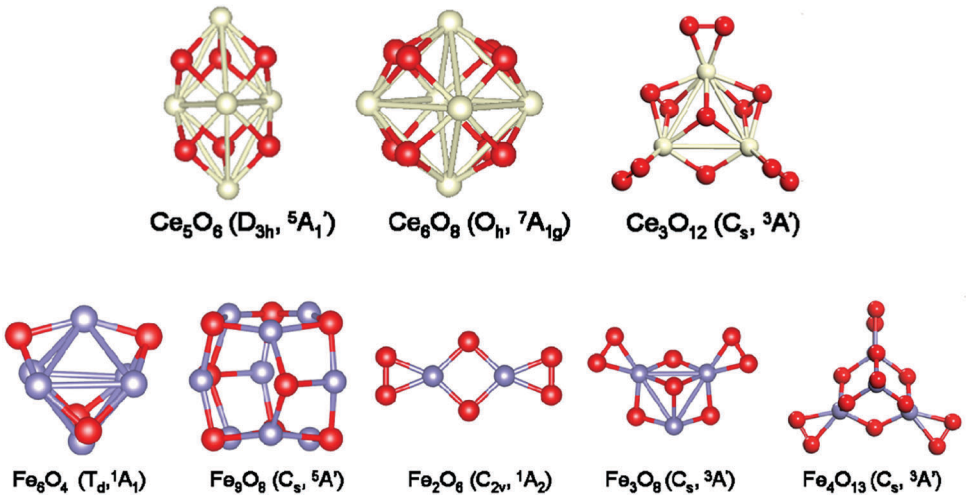

Fig. 6 Representative examples of doubly magic non-stoichiometric clusters: metal-rich Ce_5O_6, Ce_6O_8, Fe_6O_4 and Fe_9O_8, and oxygen-rich Ce_3O_{12}, Fe_3O_8 and Fe_4O_{13}. Metal-rich clusters feature metal–metal bonds (which can be delocalized over the entire cluster, as in Ce_6O_8[57]), while oxygen-rich (superoxidized) clusters feature O–O bonds in peroxo- and superoxo-groups.

Similar to Ce_mO_n clusters, some magic clusters Fe_mO_n are determined by geometry, either deriving from the bulk structure or other high-symmetry atomic arrangements with filled geometric shells. For example, the following magic clusters have structures different from the bulk, but with high symmetry: Fe_6O_4, Fe_7O_5, Fe_8O_5, Fe_8O_{14}, Fe_9O_6, and Fe_9O_8 (Fig. S7, ESI†). The doubly magic cluster Fe_9O_6 is in agreement with previous theoretical and experimental reports.[61] Among the clusters with higher oxygen concentration, Fe_2O_6, Fe_3O_8 and Fe_4O_{13} clusters have both large Δ^2F_m and Δ^2F_n, and are therefore doubly magic clusters as well. Structures of some non-stoichiometric doubly magic Fe_mO_n and Ce_mO_n clusters are shown in Fig. 6. Suboxide clusters (with Fe/O $>$ 1 and Ce/O $>$ 2/3) typically feature (often multicenter) metal–metal bonds and can be expected to be excellent reducing agents. Superoxidized clusters (Fe/O $<$ 2/3 and Ce/O $<$ 1/2) feature O–O bonds and should be powerful oxidants; these are predicted to be abundant at room temperature and atmospheric oxygen pressure in Ce_mO_n and Fe_mO_n (Fig. 1), a situation recently discovered for Si_mO_n clusters,[56] and probably typical of most oxide clusters, and due to the presence of reactive oxygen species (peroxide, superoxide and ozonide groups) such clusters can display biotoxicity and carcinogenicity (Si_mO_n,[56] and Ti_mO_n[62]).

To summarize, we employed the state-of-the-art evolutionary structure prediction algorithm USPEX, DFT+U calculations, and *ab initio* thermodynamics to study transition metal oxide clusters. For the first time, we systematically investigated magic clusters in such systems and singled out those compositions which become "magic" (*i.e.* conditionally thermodynamically stable) at a given temperature and oxygen pressure. We found that the most stable stoichiometric Ce_nO_{2n} clusters have a closed-shell electronic configuration (singlet), in contrast to nonstoichiometric Ce_nO_{2n-x} clusters: for example, Ce_nO_{2n-1} clusters have triplet state with the magnetic moment localized on the Ce atoms reduced from Ce^{4+} to Ce^{3+}. This suggests the possibility of tuning the magnetic properties by changing partial oxygen pressure and temperature. For Fe_mO_n clusters, all Fe_m clusters are ferromagnetic, low-oxygen Fe_mO_n clusters are ferri- or antiferromagnetic, and high-oxygen Fe_mO_n clusters are all antiferromagnetic when m = even and ferrimagnetic when m = odd. This indicates that a competition between ferromagnetism (induced by direct exchange) and antiferromagnetism (induced by superexchange or double exchange) plays an important role in determining the stability of low-oxygen Fe_mO_n clusters. At high partial pressures of oxygen, dominant magic nanoparticles contain excess oxygen as peroxide and superoxide groups attached to their surface. We can also notice that magic clusters form ridges and islands of stability, surrounded by the "sea of instability" in the compositional space – a picture very similar to what is found for atomic nuclei (which can also be described as clusters made of two types of particles, protons and neutrons). We expect that the topology of the ridges and islands of stability should be an important factor determining the feasibility or infeasibility of a particular chemical transformation of a nanoparticle.

Conflicts of interest

The authors declare no competing financial interest.

Acknowledgements

A. R. O. acknowledges funding from the Russian Science Foundation (grant 16-13-10459). X. H. Y. acknowledges funding from the National Science Foundation of Henan Province (grant no. 162300410001), the Natural Science Foundation of Shaanxi University of Technology (no. SLGQD1809), team of syngas catalytic conversion of Shaanxi University of Technology, and the Special Funding for Transformation of Scientific and Technological Achievements in Qinghai Province (no. 2018-GX-101).

References

1 C. Binns, *Surf. Sci. Rep.*, 2001, **44**, 1–49.
2 F. Baletto and R. Ferrando, *Rev. Mod. Phys.*, 2005, **77**, 371–423.
3 S. N. Khanna and P. Jena, *Phys. Rev. Lett.*, 1992, **69**, 1664–1667.
4 O. Echt, K. Sattler and E. Recknagel, *Phys. Rev. Lett.*, 1981, **47**, 1121–1124.
5 W.-D. Knight, K. Clemenger, W. A. de Heer, W. A. Saunders, M. Chou and M. L. Cohen, *Phys. Rev. Lett.*, 1984, **52**, 2141–2143.
6 J. U. Reveles, P. A. Clayborne, A. C. Reber, S. N. Khanna, K. Pradhan, P. Sen and M. R. Pederson, *Nat. Chem.*, 2009, **1**, 310–315.
7 X. Li, A. E. Kuznetsov, H.-F. Zhang, A. I. Boldyrev and L.-S. Wang, *Science*, 2001, **291**, 859–861.
8 X. Yu, A. R. Oganov, I. A. Popov, G. Qian and A. I. Boldyrev, *Angew. Chem., Int. Ed.*, 2016, **55**, 1699–1703.
9 X. Yu, X. Zhang and X.-W. Yan, *Nano Res.*, 2018, **11**, 3574–3581.
10 S. F. Li, H. Lu, P. Li, Z. Yang and Z. X. Guo, *J. Chem. Phys.*, 2008, **128**, 164718.
11 D. Mei and Q. Ge, *Comput. Theor. Chem.*, 2012, **987**, 25–31.
12 C. Chen, H.-L. Chen, M.-H. Weng, S.-P. Ju, J.-G. Chang and C.-S. Chang, *Chin. J. Catal.*, 2008, **29**, 1117–1121.
13 H.-L. Chen, M.-H. Weng, S.-P. Ju, J.-G. Chang, H.-T. Chen and C.-S. Chang, *J. Mol. Struct.*, 2010, **963**, 2–8.
14 H. Shiroishi, T. Oda, I. Hamada and N. Fujima, *Eur. Phys. J. D*, 2003, **24**, 85–88.
15 H. Wu, S. R. Desai and L.-S. Wang, *J. Am. Chem. Soc.*, 1996, **118**, 5296–5301.
16 L.-S. Wang, H. Wu and S. R. Desai, *Phys. Rev. Lett.*, 1996, **76**, 4853–4856.
17 A. Kirilyuk, A. Fielicke, K. Demyk, G. von Helden, G. Meijer and T. Rasing, *Phys. Rev. B: Condens. Matter Mater. Phys.*, 2010, **82**, 020405.
18 B. V. Reddy and S. N. Khanna, *Phys. Rev. Lett.*, 2004, **93**, 068301.
19 G. L. Gutsev, S. N. Khanna, B. K. Rao and P. Jena, *Phys. Rev. A: At., Mol., Opt. Phys.*, 1999, **59**, 3681–3684.
20 N. O. Jones, B. V. Reddy, F. Rasouli and S. N. Khanna, *Phys. Rev. B: Condens. Matter Mater. Phys.*, 2005, **72**, 165411.
21 X.-L. Ding, W. Xue, Y.-P. Ma, Z.-C. Wang and S.-G. He, *J. Chem. Phys.*, 2009, **130**, 014303.
22 A. Erlebach, C. Huhn, R. Jana and M. Sierka, *Phys. Chem. Chem. Phys.*, 2014, **16**, 26421–26426.
23 A. Erlebach, H.-D. Kurland, J. Grabow, F. A. Muller and M. Sierka, *Nanoscale*, 2015, **7**, 2960–2969.
24 S. López, A. H. Romero, J. Mejía-López, J. Mazo-Zuluaga and J. Restrepo, *Phys. Rev. B: Condens. Matter Mater. Phys.*, 2009, **80**, 085107.
25 K. Palotás, A. N. Andriotis and A. Lappas, *Phys. Rev. B: Condens. Matter Mater. Phys.*, 2010, **81**, 075403.
26 A. R. Oganov and C. W. Glass, *J. Chem. Phys.*, 2006, **124**, 244704.
27 W. Zhang, A. R. Oganov, A. F. Goncharov, Q. Zhu, S. E. Boulfelfel, A. O. Lyakhov, E. Stavrou, M. Somayazulu, V. B. Prakapenka and Z. Konôpková, *Science*, 2013, **342**, 1502–1505.
28 X.-F. Zhou, X. Dong, A. R. Oganov, Q. Zhu, Y. Tian and H.-T. Wang, *Phys. Rev. Lett.*, 2014, **112**, 085502.
29 A. R. Oganov, A. O. Lyakhov and M. Valle, *Acc. Chem. Res.*, 2011, **44**, 227–237.
30 A. O. Lyakhov, A. R. Oganov, H. T. Stokes and Q. Zhu, *Comput. Phys. Commun.*, 2013, **184**, 1172–1182.
31 Q. Zhu, V. Sharma, A. R. Oganov and R. Ramprasad, *J. Chem. Phys.*, 2014, **141**, 154102.
32 G. Kresse and D. Joubert, *Phys. Rev. B: Condens. Matter Mater. Phys.*, 1999, **59**, 1758–1775.
33 G. Kresse and J. Furthmüller, *Phys. Rev. B: Condens. Matter Mater. Phys.*, 1996, **54**, 11169–11186.
34 S. L. Dudarev, G. A. Botton, S. Y. Savrasov, C. J. Humphreys and A. P. Sutton, *Phys. Rev. B: Condens. Matter Mater. Phys.*, 1998, **57**, 1505–1509.
35 Z. Yang, X. Yu, Z. Lu, S. Li and K. Hermansson, *Phys. Lett. A*, 2009, **373**, 2786–2792.
36 X. Yu, X. Zhang, L. Jin and G. Feng, *Phys. Chem. Chem. Phys.*, 2017, **19**, 17287–17299.
37 X. Yu, S.-G. Wang, Y.-W. Li, J. Wang and H. Jiao, *J. Phys. Chem. C*, 2012, **116**, 10632–10638.
38 X. Yu, C.-F. Huo, Y.-W. Li, J. Wang and H. Jiao, *Surf. Sci.*, 2012, **606**, 872–879.
39 H. J. Kulik, M. Cococcioni, D. A. Scherlis and N. Marzari, *Phys. Rev. Lett.*, 2006, **97**, 103001.
40 J. Heyd, G. E. Scuseria and M. Ernzerhof, *J. Chem. Phys.*, 2003, **118**, 8207–8215.
41 J. Heyd and G. E. Scuseria, *J. Chem. Phys.*, 2004, **121**, 1187–1192.
42 O. A. Vydrov, J. Heyd, A. V. Krukau and G. E. Scuseria, *J. Chem. Phys.*, 2006, **125**, 074106.
43 Y. Meng, X.-W. Liu, C.-F. Huo, W.-P. Guo, D.-B. Cao, Q. Peng, A. Dearden, X. Gonze, Y. Yang, J. Wang, H. Jiao, Y. Li and X.-D. Wen, *J. Chem. Theory Comput.*, 2016, **12**, 5132–5144.
44 S. Bhattacharya, S. V. Levchenko, L. M. Ghiringhelli and M. Scheffler, *Phys. Rev. Lett.*, 2013, **111**, 135501.
45 E. C. Beret, M. M. van Wijk and L. M. Ghiringhelli, *Int. J. Quantum Chem.*, 2013, **114**, 57–65.
46 X. Yu, X. Zhang, H. Wang, Z. Wang and G. Feng, *J. Phys. Chem. C*, 2017, **121**, 22081–22091.
47 X. Yu, X. Zhang, Y. Meng, Y. Zhao, Y. Li, W. Xu and Z. Liu, *Appl. Surf. Sci.*, 2018, **434**, 464–472.
48 D. R. Stull and H. Prophet, JANAF thermochemical tables; U. S. National Bureau of Standards: U. S. EPO, Washington D. C, DTIC Document, 1971.
49 S. Yin, W. Xue, X.-L. Ding, W.-G. Wang, S.-G. He and M.-F. Ge, *Int. J. Mass Spectrom.*, 2009, **281**, 72–78.
50 D. N. Shin, Y. Matsuda and E. R. Bernstein, *J. Chem. Phys.*, 2004, **120**, 4150–4156.
51 D. N. Shin, Y. Matsuda and E. R. Bernstein, *J. Chem. Phys.*, 2004, **120**, 4157–4164.
52 K. S. Molek, C. Anfuso-Cleary and M. A. Duncan, *J. Phys. Chem. A*, 2008, **112**, 9238–9247.
53 W. Geertsma, *Phys. B*, 1990, **164**, 241–260.
54 B. Bechlars, D. M. D'Alessandro, D. M. Jenkins, A. T. Iavarone, S. D. Glover, C. P. Kubiak and J. R. Long, *Nat. Chem.*, 2010, **2**, 362–368.

55 G. L. Gutsev, C. A. Weatherford, K. Pradhan and P. Jena, *J. Phys. Chem. A*, 2010, **114**, 9014–9021.
56 S. Lepeshkin, V. Baturin, E. Tikhonov, N. Matsko, Y. Uspenskii, A. Naumova, O. Feya, M. A. Schoonen and A. R. Oganov, *Nanoscale*, 2016, **8**, 18616–18620.
57 X. Yu, A. R. Oganov, I. A. Popov and A. I. Boldyrev, *J. Comput. Chem.*, 2016, **37**, 103–109.
58 Z. L. Wang and X. Feng, *J. Phys. Chem. B*, 2003, **107**, 13563–13566.
59 M. R. Pederson and S. N. Khanna, *Phys. Rev. B: Condens. Matter Mater. Phys.*, 1999, **59**, R693–R696.
60 M. R. Pederson, F. Reuse and S. N. Khanna, *Phys. Rev. B: Condens. Matter Mater. Phys.*, 1998, **58**, 5632–5636.
61 Q. Sun, M. Sakurai, Q. Wang, J. Z. Yu, G. H. Wang, K. Sumiyama and Y. Kawazoe, *Phys. Rev. B: Condens. Matter Mater. Phys.*, 2000, **62**, 8500–8507.
62 S. Bettini, E. Boutet-Robinet, C. Cartier, C. Coméra, E. Gaultier, J. Dupuy, N. Naud, S. Taché, P. Grysan, S. Reguer, N. Thieriet, M. Réfrégiers, D. Thiaudière, J.-P. Cravedi, M. Carrière, J.-N. Audinot, F. H. Pierre, L. Guzylack-Piriou and E. Houdeau, *Sci. Rep.*, 2017, **7**, 40373.

